Revisiting Molecularly Conformation-Planarized Organic Dyes for NIR-II Fluorescence Imaging

Lei An,[a] Liangyu Zheng,[a] Ziqi Zhao,[a] Xinyu Qu,[b] Chen liang,[d] Changjin Ou, *[a] Xiaozhou Mou,[d] Xiaochen Dong*[b,c], Yu Cai*[d]

[a]Institute of Advanced Materials and Flexible Electronics (IAMFE), School of Chemistry and Materials Science, Nanjing University of Information Science & Technology, Nanjing 210044, China

E-mail: 003239@nuist.edu.cn

[b]Key Laboratory of Flexible Electronics (KLOFE) & Institute of Advanced Materials (IAM), Nanjing Tech University (NanjingTech), Nanjing 211816, China

[c]School of Chemistry & Materials Science, Jiangsu Normal University, Xuzhou 221116, China

E-mail: iamxcdong@njtech.edu.cn

[d]Center for Rehabilitation Medicine, Rehabilitation & Sports Medicine Research Institute of Zhejiang Province Department of Rehabilitation Medicine, Zhejiang Provincial People's Hospital Affiliated People's Hospital, Hangzhou Medical College, Hangzhou, Zhejiang 310014, China

E-mail: caiyu@hmc.edu.cn

1 General information and methods

1.1 Materials

All chemicals were purchased from Energy-Chemical Co. Ltd., and the solvents for chemical reactions were used without purification unless otherwise stated. All oxygen and moisture-sensitive reactions were carried out in flame-dried glassware under N_2 atmosphere. RPMI 1640 Medium cell cultures were purchased from Adamas Co. Ltd. DSPE-PEG2000 was purchased from Bidepharm Co. Ltd.

1.2 Measurements

^{1}H and ^{13}C-NMR spectra were measured on 400 MHz NMR spectrometers (JEOL 400YH) using $CDCl_3$ as a deuterated solvent and tetramethylsilane (TMS) as an internal standard. UV-vis absorption and NIR-II fluorescence spectra were measured in an organic solvent or aqueous solution using a SHIMADZY UV-3600 plus spectrophotometer and Edinburgh FLS980 spectrophotometer, respectively. The size and scale were measured via transmission electron microscopy (TEM, JEM-2010FEF) and dynamic light scattering (DLS). In vitro and vivo NIR-II fluorescence imaging was performed with a small animal imaging system (Suzhou NIR-Optics, China) equipped with long-pass filters. Cytotoxicity was determined by a multifunctional microplate reader (Varioskan LUX)

1.3 Fabrication of NIR-II NPs with different doping concentrations

In a general procedure, matrix DBT (40 mg) and NIR-II molecule T-BBT or BT-BBT (7 mg) were dissolved in tetrahydrofuran with concentrations of 10 mg/mL and 3.5 mg/mL, respectively. According to the configuration shown in the Table S2, the matrix and NIR-II dye solution were placed into a centrifuge tube and DSPE-PEG2000 (25 mg) was added to each tube. In the end, the mixture was slowly injected into water (6 mL), and the THF was evaporated under reduced pressure at 40℃.

1.4 Calculation of relative fluorescence photoluminescence quantum yield (PLQY)

The PLQYs were measured in a similar way to the previous report, using fluorescent dye FT-BBT as a reference fluorophore (PLQY = 19% in toluene).[1] First, for the reference calibration, FT-BBT dissolved in toluene to prepare five samples (1, 2, 3, 4, 5 ug/mL) with 808 nm absorbance values of about 0.01-0.15. Second, T-BBT and BT-BBT were dissolved in dichloromethane (DCM) with different concentrations (1, 2, 3, 4, and 5 μg/mL), and DT-BBT 2.5 wt% NPs and DBT-BBT 2.5 wt% NPs were dispersed in water with different concentrations (40, 60, 80, 100, and 120 μg/mL), and the 808 nm absorbance of the four materials mentioned above were less than 0.1. Then, the concentrations were plotted against absorbance at 808 nm and fitted into a linear function. Finally, five linear functions were constructed by Origin 2022b via the same procedures, and the corresponding slope could be calculated as the quantum yield of the sample based on the following equation:

$$\Phi_{sample} = \Phi_{FT\text{-}BBT} \times \frac{Slope_{sample}}{Slope_{FT\text{-}BBT}} \times \frac{n_{sample}^2}{n_{toluene}^2}$$

where n is the refractive index of the dispersion medium ($^{n}_{toluene}$ = 1.4962, $^{n}_{DCM}$ = 1.4242, $^{n}_{water}$=1.333). Related data were summarized in Table S3.

1.5 Solvatochromic effect

Interactions between solvents and fluorescent molecules have influence on the energy gap between ground and excited states. This effect can be quantified by dielectric constant (ε), refractive index (n) according to the Lippert-Mataga equation:

$$\bar{v}_{abs} - \bar{v}_{em} = \frac{2(\mu_E - \mu_G)^2}{hca^3}\Delta f + Const.$$

where $\bar{v}_{abs}$ and $\bar{v}_{em}$ are the peaks of absorption and emission, respectively; and μ_E and μ_G are the dipole moment of ground and excited states, respectively; h, c, and a are the Planck constant,

light velocity, and the radius of the Onsager cavity, respectively; and Δf, solvent orientation polarizability, can be calculated by following equation:

$$\Delta f = \frac{(\varepsilon - 1)}{(2\varepsilon + 1)} - \frac{(n^2 - 1)}{(2n^2 + 1)}$$

where ε is dielectric constant and n is refractive index of solvent. Herein, the slope of linear fitting line between Stokes shift (Δv) and Δf can be used to evaluate the difference of dipole moments between ground state and excited state.

1.6 Interaction type factor

Multipolar interaction type can be determined by the following formula: [2]

$$\frac{I}{x} = k[1 + \beta(x)^{\theta/3}]^{-1}$$

where I is fluorescence intensity, x is the molar fraction of dyes, k and β are constant for a given NPs in the same excitation condition. The slope -θ/3 can be calculated from the linear fitting curve between lg(x) and lg(I/x) of NPs, and therefore the interaction type factor θ obtained. The interaction type factor θ of 6 means to dipole-dipole interaction.

1.7 Particle size, zeta potential, and photostability stability studies

The particle size and zeta potential of T-BBT 2.5 wt% NPs and BT-BBT 2.5 wt% NPs were employed by DLS. Their particle sizes, variance (P.I.), and zeta potential values were measured at different time points. T-BBT 2.5 wt% NPs and BT-BBT 2.5 wt% NPs were excited under 980 nm laser (26 mW/cm^2, 200ms, LP1100), and their fluorescence images were captured by NIR fluorescence imager at different time points.

1.8 Cytotoxicity assays

4T1 murine breast cancer cells were cultured in fresh RPMI 1640 Medium containing 10% inactivated fetal bovine serum (FBS) and 1% penicillin-streptomycin at 37℃ in a 5% CO_2 humidified incubator. Cells were cultured in a 96-well plate for 24 h incubation. Then, the

medium was replaced with 200 uL of fresh RPMI 1640 containing different concentrations of 2.5% wt% DT-BBT NPs and DBT-BBT NPs (0, 20, 40, 60, 80, 100, 150, 200, 250, and 300 μg/mL) for 24 h in the incubator, the number of the well is five for each group. To evaluate the cytotoxicity, the MTT solution (20 μL, 5mg/mL) was added to each well of the microliter plate and the plate was incubated in the incubator for an additional 4 h. Finally, the 200 μL DMSO was added to dissolve the purple precipitate after removing the culture medium. The absorbance was measured at the optical densities (O.D.) of 492 nm with a multifunctional microplate reader. Each group had 3 repetitions.

The following formula was employed to calculate the cell viability:

Cell Viability (%) = (absorbance of experimental group/the absorbance of the control group) × 100%

1.9 *In vivo* fluorescence imaging

All animal experiments were approved and guided by the School of Pharmaceutical Science, Nanjing Tech University, in compliance with the relevant laws and institutional guidelines. The nude mice were purchased from the Comparative Medicine Centre of Yangzhou University. The mice were anesthetized before imaging. The whole-body vessel and hindlimb imaging of mice, 200 μL, 2.0 mg/mL (2.5 wt%) BT-BBT was intravenously injected into the mice's blood vessels. The administered mice were excited with 980 nm laser at NIR-II fluorescence imaging system, experiment conditions: 1100 nm long-pass filter, energy fluence (120 mW/cm^2), and exposure time (300 ms).

For the tumor imaging of balb/c mice, 150 μL, 2.0 mg/mL (2.5 wt%) BT-BBT was intravenously injected into the mice's blood vessels. The administered mice were excited with 980 nm laser at NIR-II fluorescence imaging system, experiment conditions: 1100 nm long-pass filter, energy fluence (100 mW/cm^2), and exposure time (200 ms). The fluorescence images were

captured at 0, 4, 8, 12, 24, 48, and 96 h post-injection. To check the in vivo biosafety of BT-BBT doped NPs, the mouse was sacrificed after 96 h post-injection, and the major organs (including the heart, liver, spleen, lung, and kidney) for hematoxylin and eosin (H&E) staining.

2 Synthesis and characterization

2.1 Synthesis and characterization of T-BBT

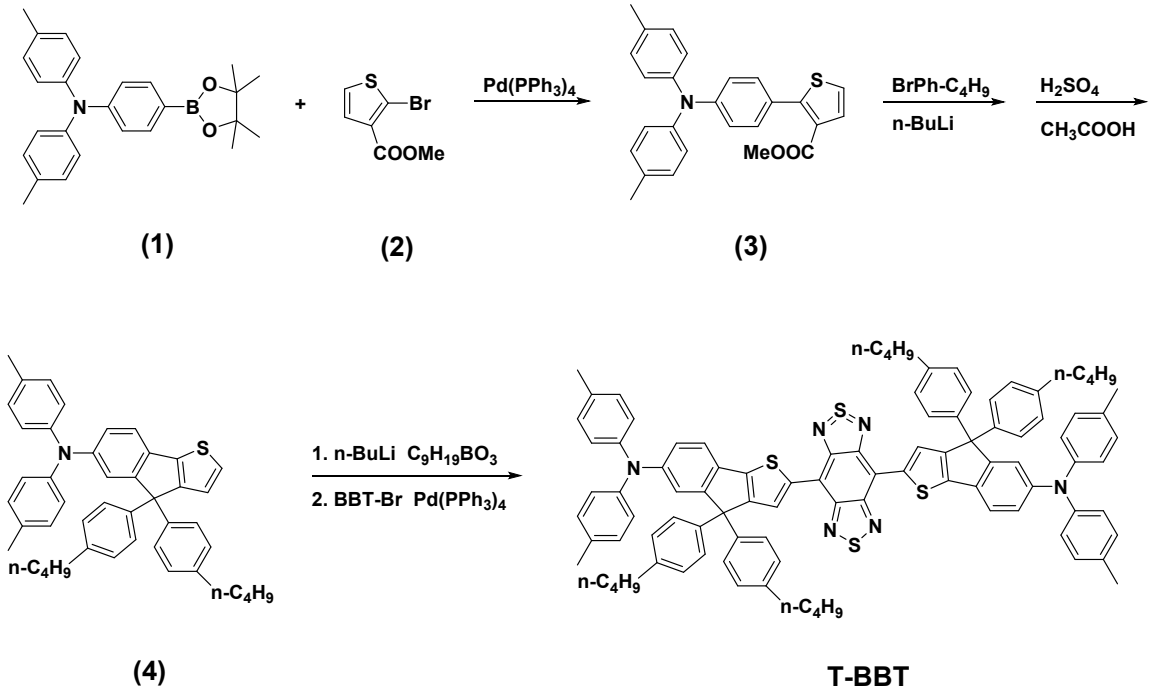

Scheme S1. Synthetic routes to DT-BBT

Synthesis of compound 3. Compound 1 (2.5 g, 6.4 mmol), compound 2 (0.9 g, 4.2 mmol), $Pd(PPh_3)_4$ (0.24 g, 0.2 mmol) and K_2CO_3/KF (2M, 4.2 mL) in THF/Tol (20 mL/20 mL) was stirred at 90°C under N_2 in dark. After 24 h, the mixture was extracted with DCM, the organic phase was dried over $MgSO_4$ and concentrated. The residue was purified by silica gel column chromatography to afford compound 4 as the light-yellow solid (1.3 g, 3 mmol, 76%). ^{1}H NMR

(400 MHz, Chloroform-*d*) δ 7.52 – 7.43 (m, 1H), 7.36 – 7.29 (m, 2H), 7.20 – 7.14 (m, 1H), 7.12 – 7.02 (m, 8H), 7.02 – 6.94 (m, 2H), 3.76 (s, 3H), 2.33 (s, 6H). ^{13}C NMR (100 MHz, Chloroform-*d*) δ 164.53, 152.35, 149.09, 145.30, 133.57, 130.83, 130.44, 130.40, 127.08, 125.71, 125.65, 123.63, 120.83, 51.54, 20.70.

Synthesis of compound 4. n-BuLi (1.6 M, 9 mL, 14 mmol) was added dropwise to 1-bromo-4-butylbenzene (3.3 g, 15 mmol) in dried THF (15 mL) at -70℃ under N_2. Compound 3 (1.5 g, 3.6 mmol) in dried THF (15 mL) was injected into the reaction system and then transferred to room temperature for 1 h. Ammonium chloride solution was added to the reaction to terminate the reaction in 10 h and then the mixture was extracted with DCM. The organic phase was dried with $MgSO_4$ and concentrated. The crude was purified by silica gel column chromatography to afford the light-yellow solid (2.2 g, 3.4 mmol, 93%). Next, the light-yellow solid (1 g, 1.5 mmol) in CH_3COOH was stirred at 110℃ and two drops of H_2SO_4 were added to it. The reaction was poured into the water for 20 min and the cyan solid was precipitated. Finally, the product (0.69 g, 1.1 mmol, 70%) was obtained by suction filtration. ^{1}H NMR (400 MHz, Chloroform-*d*) δ 7.29 (d, *J* = 0.6 Hz, 0H), 7.24 – 7.18 (m, 2H), 7.15 (d, *J* = 2.1 Hz, 1H), 7.09 – 7.03 (m, 5H), 7.01 – 6.97 (m, 8H), 6.97 – 6.91 (m, 5H), 6.89 – 6.84 (m, 1H), 2.59 – 2.51 (m, 4H), 2.29 (s, 6H), 1.59 – 1.53 (m, 4H), 1.34 (q, *J* = 14.7, 7.4 Hz, 4H), 0.92 (t, *J* = 7.3 Hz, 6H). ^{13}C NMR (100 MHz, CHLOROFORM-*d*) δ 155.63, 155.44, 146.56, 145.86, 142.56, 141.55, 141.43, 132.53, 131.72, 130.13, 128.55, 128.21, 127.02, 124.50, 123.59, 122.43, 122.12, 119.91, 62.89, 35.11, 33.47, 22.28, 20.64, 13.79.

Synthesis of compound T-BBT. n-BuLi (1.6 M, 0.82 mL, 1.3 mmol) was added dropwise to compound 4 (0.55 g, 8.7 mmol) in dried THF (15 mL) at -30℃ under N_2. $C_9H_{19}BO_3$ (0.53 mL,

2.6 mmol) was injected into the reaction and then transferred to room temperature. The mixture was concentrated in 6 h. A mixture of the crude, BBT (150 mg, 4.3 mmol), $Pd(PPh_3)_4$ (98 mg, 0.9 mmol), and K_2CO_3/KF (2M, 0.9 mL) in THF/Tol (10 mL/10mL) was stirred at 90℃ under N_2 in dark. After 24 h, the reaction was extracted with DCM, and the organic layer was dried over $MgSO_4$ and concentrated. The residue was purified by silica gel column chromatography to afford T-BBT as the black powder (130 mg, 0.9 mmol, 20.8%). ^{1}H NMR (400 MHz, Chloroform-*d*) δ 7.25 – 7.21 (m, 4H), 7.10 – 7.01 (m, 36H), 2.56 (t, 8H), 2.34 (s, 12H), 1.60 – 1.49 (m, 8H), 1.40 – 1.18 (m, 8H), 0.89 (t, J = 7.3 Hz, 12H). ^{13}C NMR (100 MHz, Chloroform-*d*) δ 157.13, 150.79, 148.07, 145.99, 145.96, 145.93, 143.02, 142.79, 142.19, 141.63, 133.47, 130.82, 130.67, 129.91, 129.35, 129.26, 128.93, 125.89, 125.37, 122.71, 121.63, 121.57, 121.51, 121.49, 63.74, 35.57, 33.96, 22.68, 21.10, 14.15.

2.2 Synthesis and characterization of BT-BBT

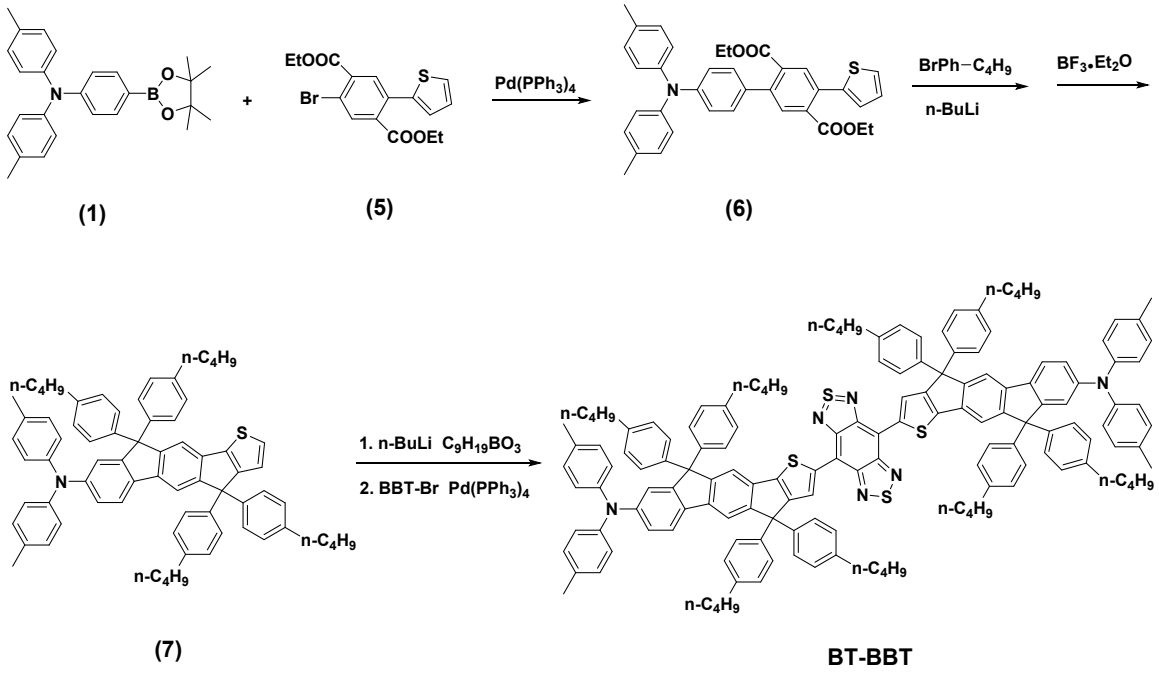

Scheme S2. Synthetic routes of BT-BBT

Synthesis of compound 6. The mixture of compound 1 (2.2 g, 5.5 mmol), compound 5 (1.4 g, 3.6 mmol), $Pd(PPh_3)_4$ (210 mg, 0.18 mmol), and K_2CO_3/KF (2 M, 3.6 mL) in THF/Tol (20 mL/20 mL) was stirred at 90℃ under N_2 in dark. The mixture was extracted with DCM, and the organic layer was dried over $MgSO_4$ and concentrated in 24 h. The residue was purified by silica gel column chromatography to afford compound 6 (1.5 g, 2.6 mmol, 70%). ^{1}H NMR (400 MHz, Chloroform-*d*) δ 7.85 (s, 1H), 7.73 (s, 1H), 7.37 (dd, *J* = 4.8, 1.6 Hz, 1H), 7.21 – 7.15 (m, 2H), 7.12 – 6.99 (m, 12H), 4.20 (q, *J* = 12.1, 7.2 Hz, 4H), 2.33 (s, 6H), 1.19 – 1.09 (m, 6H). ^{13}C NMR (100 MHz, Chloroform-*d*) δ 168.37, 168.18, 148.12, 145.21, 141.25, 140.96, 134.29, 133.41, 132.99, 132.60, 132.49, 132.31, 131.45, 130.08, 129.22, 127.41, 126.90, 126.35, 125.00, 121.86, 61.68, 61.51, 20.98, 13.96.

Synthesis of compound 7. n-BuLi (1.6 M, 9.8 mL, 15.6 mmol) was added dropwise to 1-bromo-4-butylbenzene (3.4 g, 16 mmol) in dried THF (10 mL) at -70℃ under N_2. Compound 6 (1.5 g, 2.6 mmol) in dried THF (10 mL) was injected into the reaction in 1 h and transferred to room temperature. After 24 h, the reaction was extracted with DCM, and the organic layer was dried over $MgSO_4$ and concentrated. The residue was purified by silica gel column chromatography to afford the white powder (2.36 mg, 2.3 mmol, 87.4%). Next, the white powder (2.2 g, 2.1 mmol) in DCM was stirred at room temperature, and $BF_3{\cdot}C_2H_5OC_2H_5$ was injected into it. The reaction was poured into NaOH solution for 25 min and concentrated. Compound 7 (1.1 g, 1.1 mmol, 48 %) was obtained by silica gel column chromatography. ^{1}H NMR (400 MHz, Chloroform-*d*) δ 7.59 (s, 1H), 7.44 (d, *J* = 8.3 Hz, 1H), 7.39 (s, 1H), 7.23 – 7.21 (m, 1H), 7.18 – 7.14 (m, 5H), 7.11 – 7.06 (m, 4H), 7.05 – 6.99 (m, 9H), 6.99 – 6.87 (m, 10H), 2.56 (td, *J* = 7.8, 4.1 Hz, 8H), 2.29 (s, 6H), 1.66 – 1.20 (m, 16H), 0.91 (td, *J* = 7.4, 5.7 Hz, 12H). ^{13}C NMR (100

MHz, Chloroform-*d*) δ 156.77, 154.37, 154.06, 151.72, 148.28, 146.17, 144.07, 143.13, 142.31, 142.11, 141.89, 138.75, 136.96, 134.97, 132.93, 130.51, 129.06, 129.00, 128.93, 128.72, 128.18, 124.90, 123.88, 123.05, 121.77, 120.98, 118.22, 117.91, 65.03, 63.01, 35.55, 35.52, 33.87, 22.73, 22.71, 21.04, 14.22, 14.20, 1.18.

Synthesis of BT-BBT. n-BuLi (1.6 M, 0.97 mL, 1.2 mmol) was added dropwise to compound 7 (1 g, 1 mmol) in dried THF (15 mL) at -30℃ under N_2. $C_9H_{19}BO_3$ (0.64 mL, 3 mmol) was injected into the reaction and then transferred to room temperature. The mixture was concentrated in 20 h. A mixture of the crude, BBT (150 mg, 4.3 mmol), $Pd(PPh_3)_4$ (98 mg, 0.9 mmol) and K_2CO_3/KF (2M, 0.9 mL) in THF/Tol (20 mL/20mL) was stirred at 90℃ under N_2 in dark. After 24 h, the reaction was extracted with DCM, the organic layer was dried over $MgSO_4$ and concentrated. The residue was purified by silica gel column chromatography to afford BT-BBT as the black powder (42 mg, 4.3%). ^{1}H NMR (400 MHz, Chloroform-*d*) δ 8.88 (s, 2H), 7.67 – 7.57 (m, 4H), 7.47 (d, *J* = 19.6, 8.2 Hz, 2H), 7.37 (d, *J* = 7.9 Hz, 7H), 7.22 (s, 2H), 7.19 – 7.06 (m, 17H), 7.06 – 6.99 (m, 16H), 6.98 – 6.76 (m, 14H), 2.61 – 2.51 (m, 16H), 2.39 – 2.23 (m, 12H), 1.65 – 1.23 (m, 32H), 1.11 – 0.86 (m, 24H). ^{13}C NMR (100 MHz, Chloroform-*d*) δ 158.14, 154.89, 154.12, 152.01, 148.43, 145.96, 143.86, 142.96, 142.18, 141.94, 141.77, 139.84, 136.88, 134.69, 132.90, 132.76, 130.39, 130.34, 129.17, 128.85, 128.79, 128.76, 128.55, 124.84, 124.73, 122.88, 121.51, 121.09, 118.85, 118.03, 64.92, 63.36, 35.44, 35.40, 33.79, 33.75, 29.84, 22.58, 22.52, 20.90, 14.10.

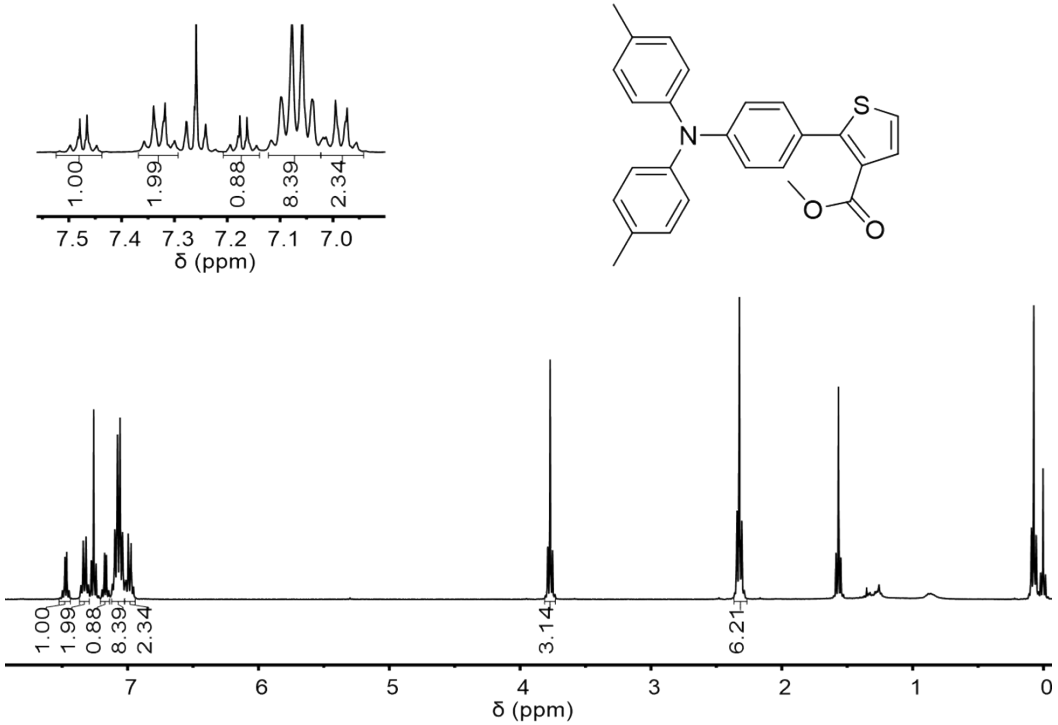

Figure S1. ^{1}H NMR spectrum of compound 3.

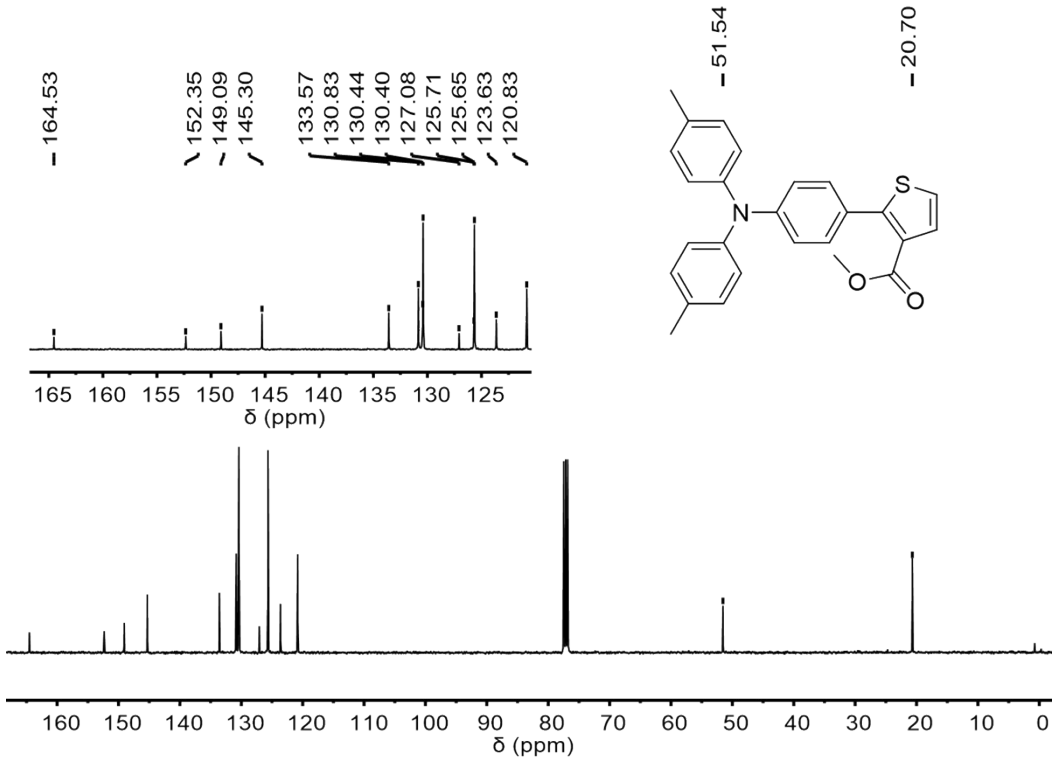

Figure S2. ^{13}C NMR spectrum of compound 3.

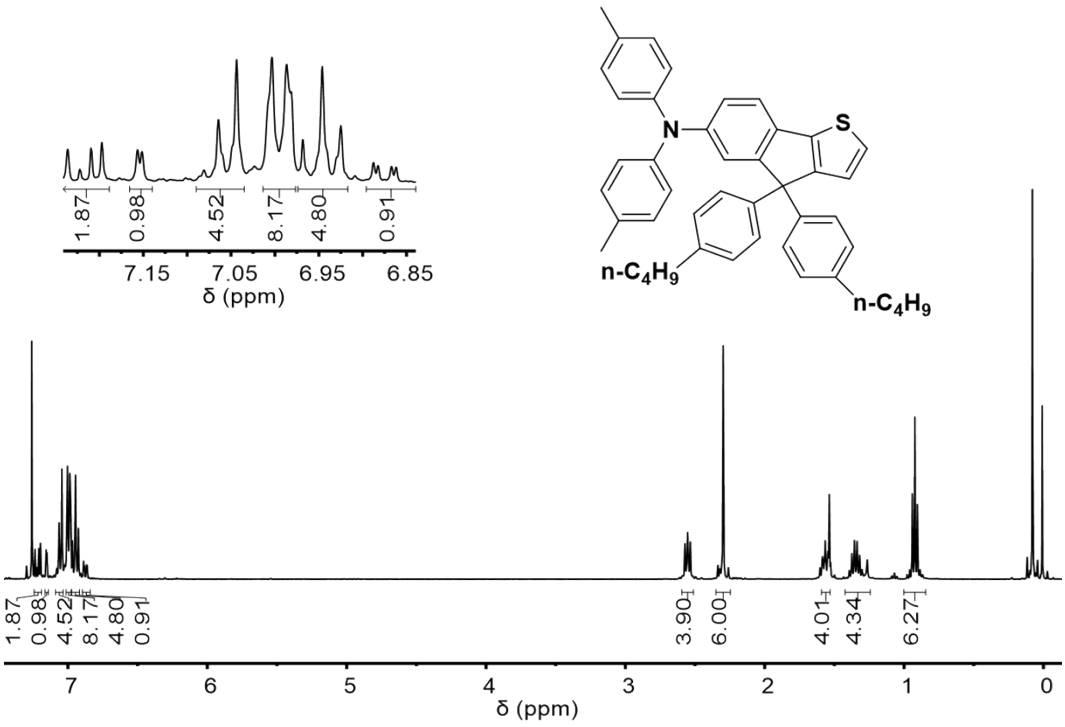

Figure S3. [1]H NMR spectrum of compound 4.

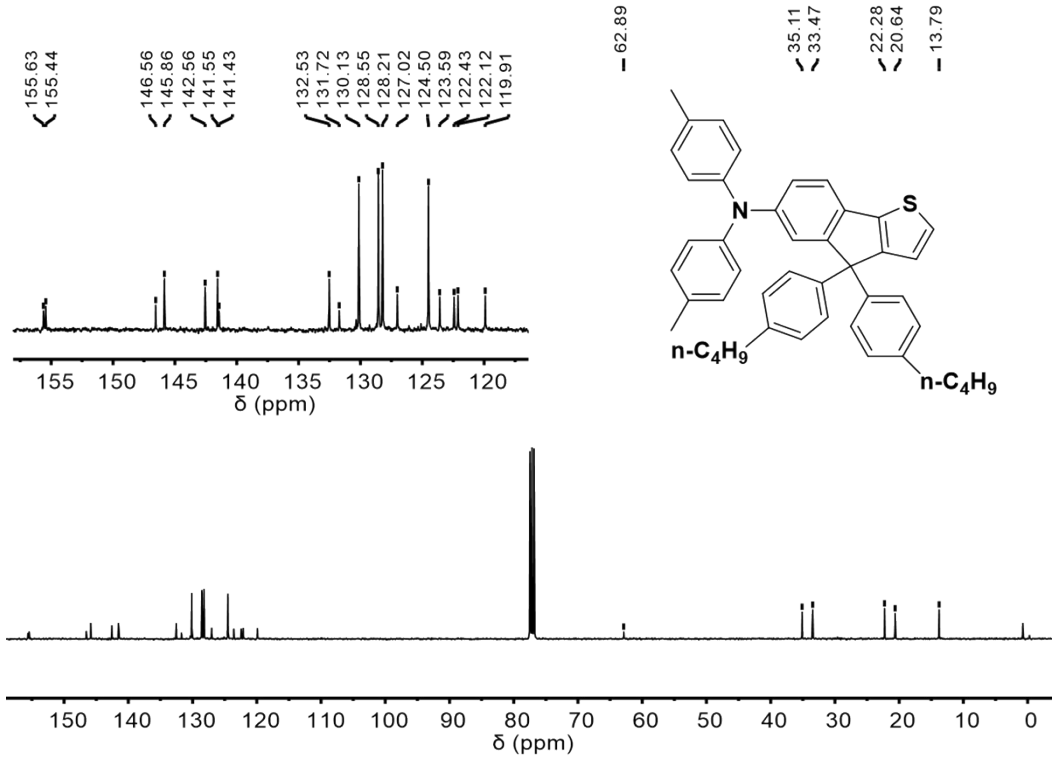

Figure S4. [13]C NMR spectrum of compound 4.

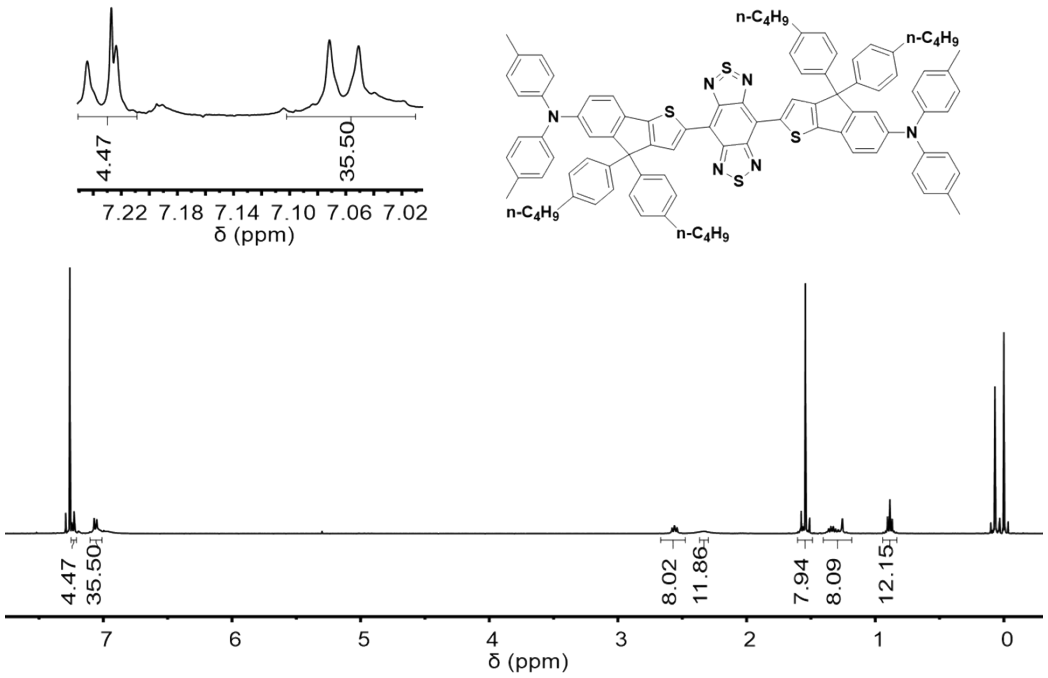

Figure S5. ^{1}H NMR spectrum of T-BBT.

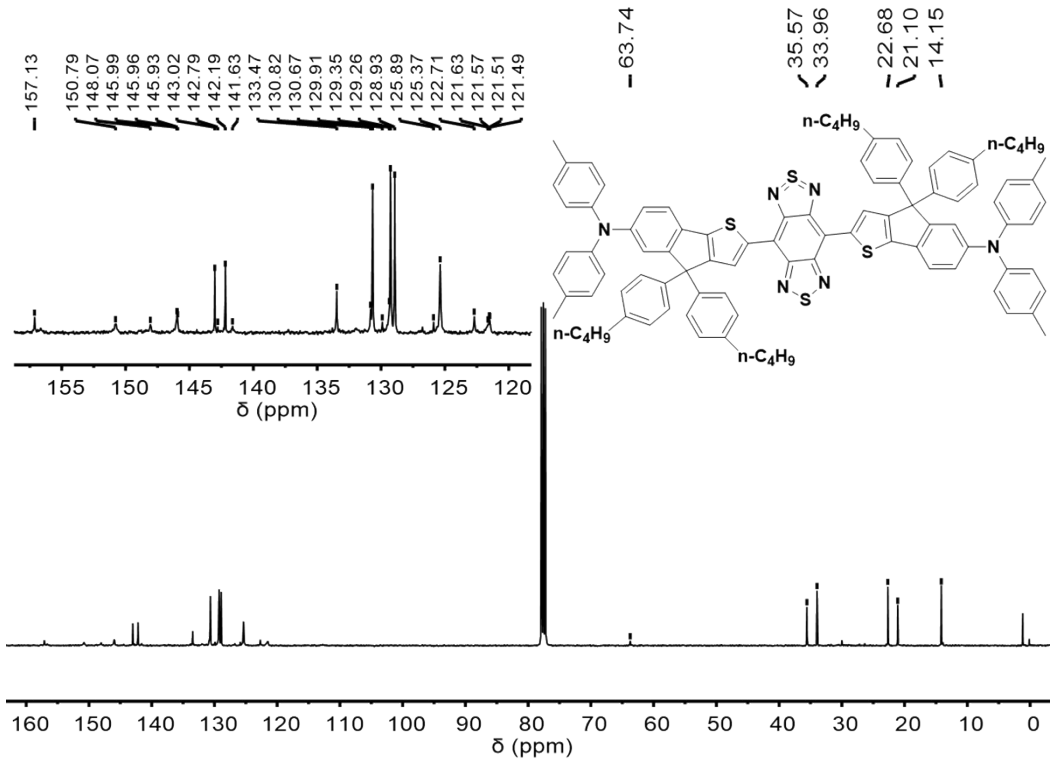

Figure S6. ^{13}C NMR spectrum of T-BBT.

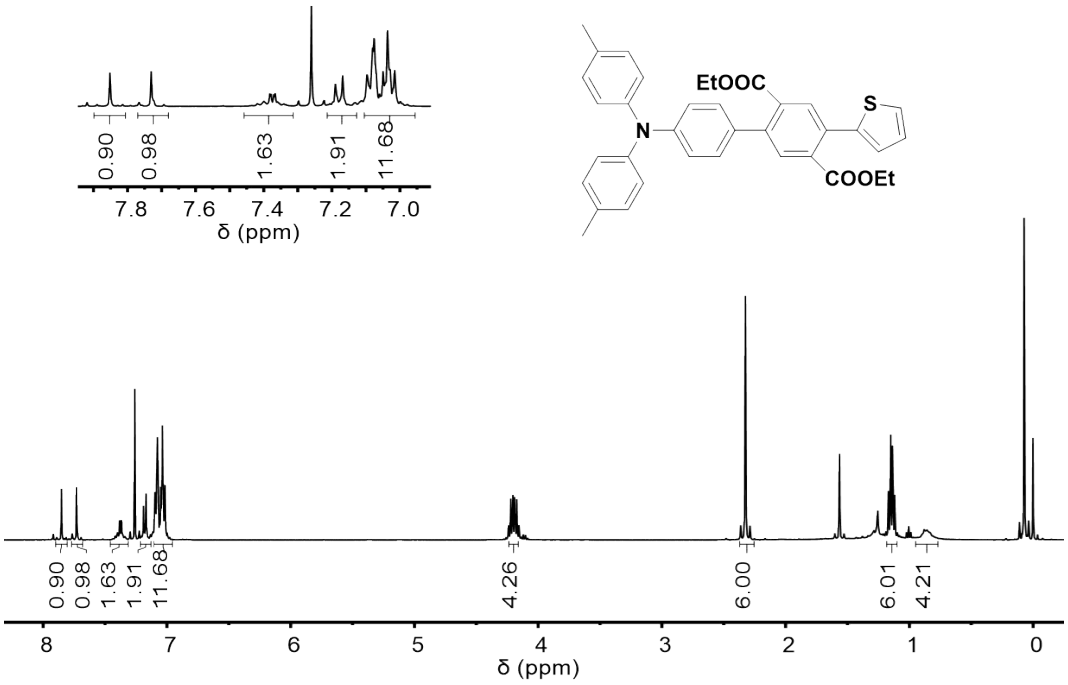

Figure S7. ^{1}H NMR spectrum of compound 6.

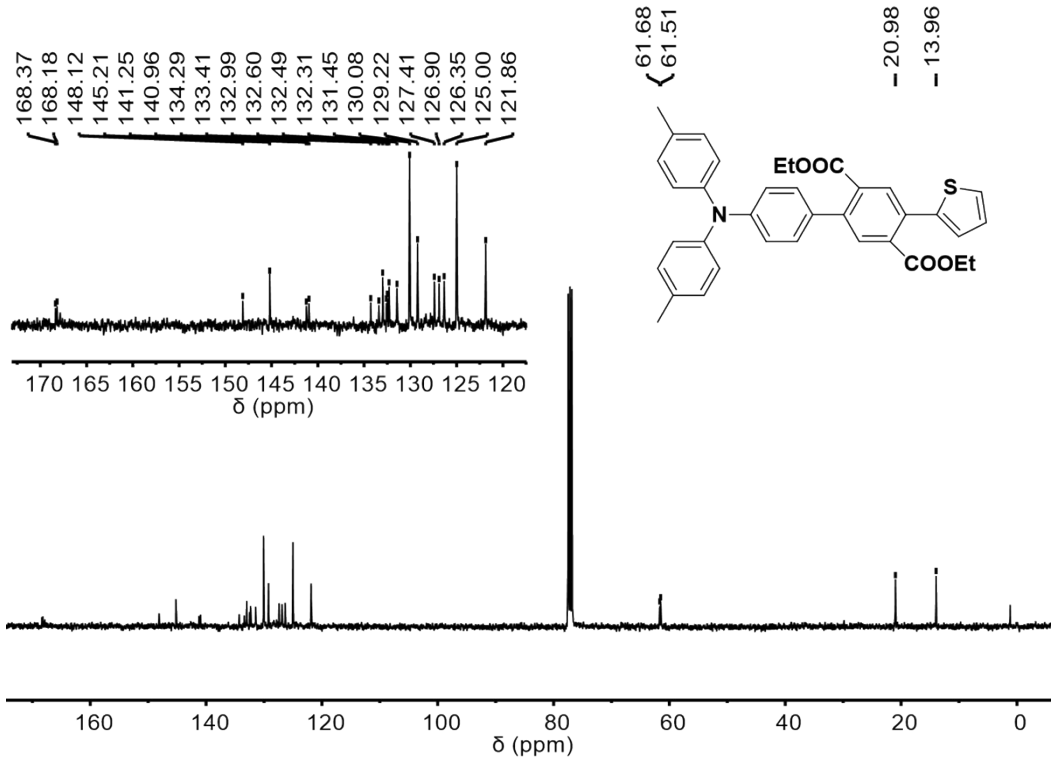

Figure S8. ^{13}C NMR spectrum of compound 6.

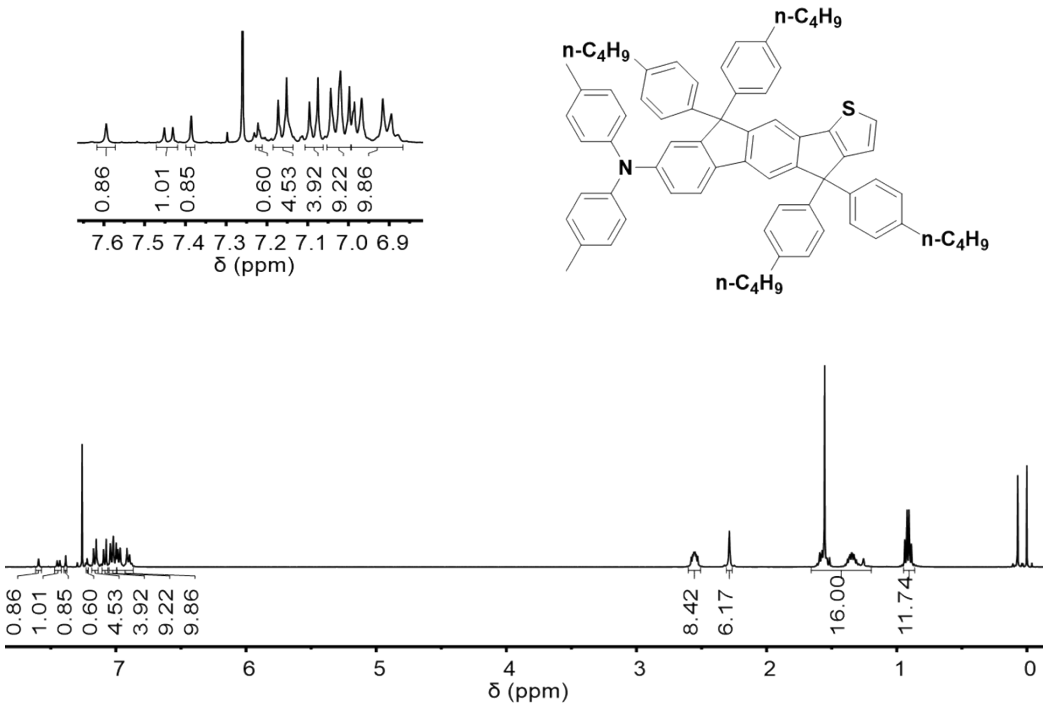

Figure S9. ^{1}H NMR spectrum of compound 7.

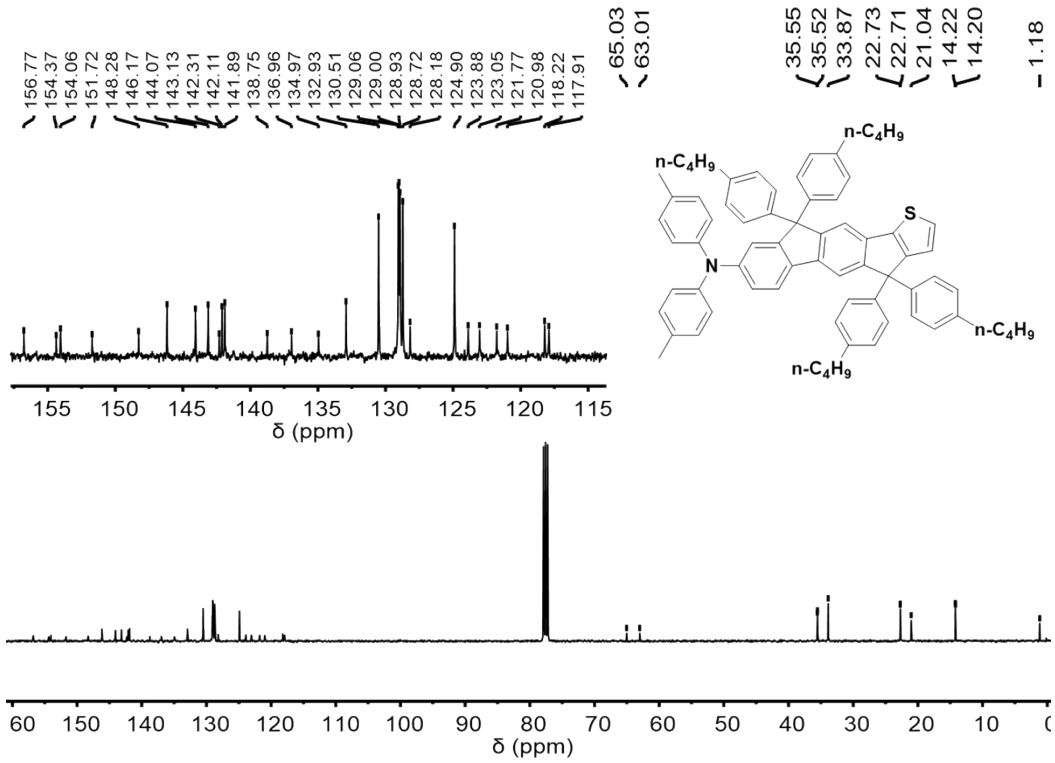

Figure S10. ^{13}C NMR spectrum of compound 7.

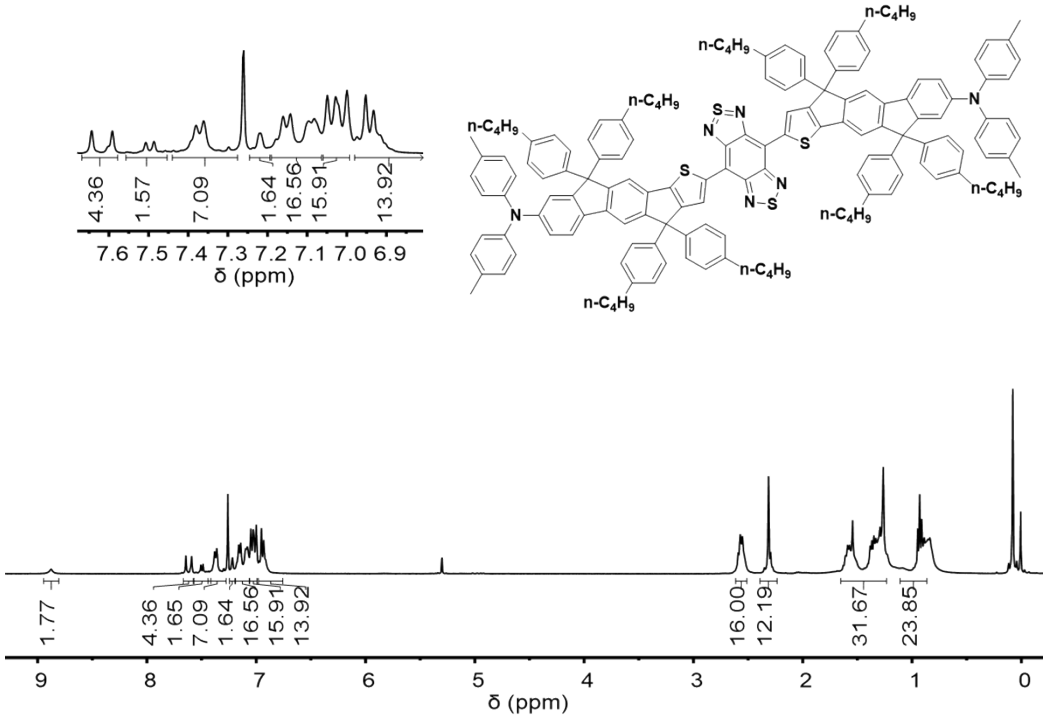

Figure S11. ^{1}H NMR spectrum of compound BT-BBT.

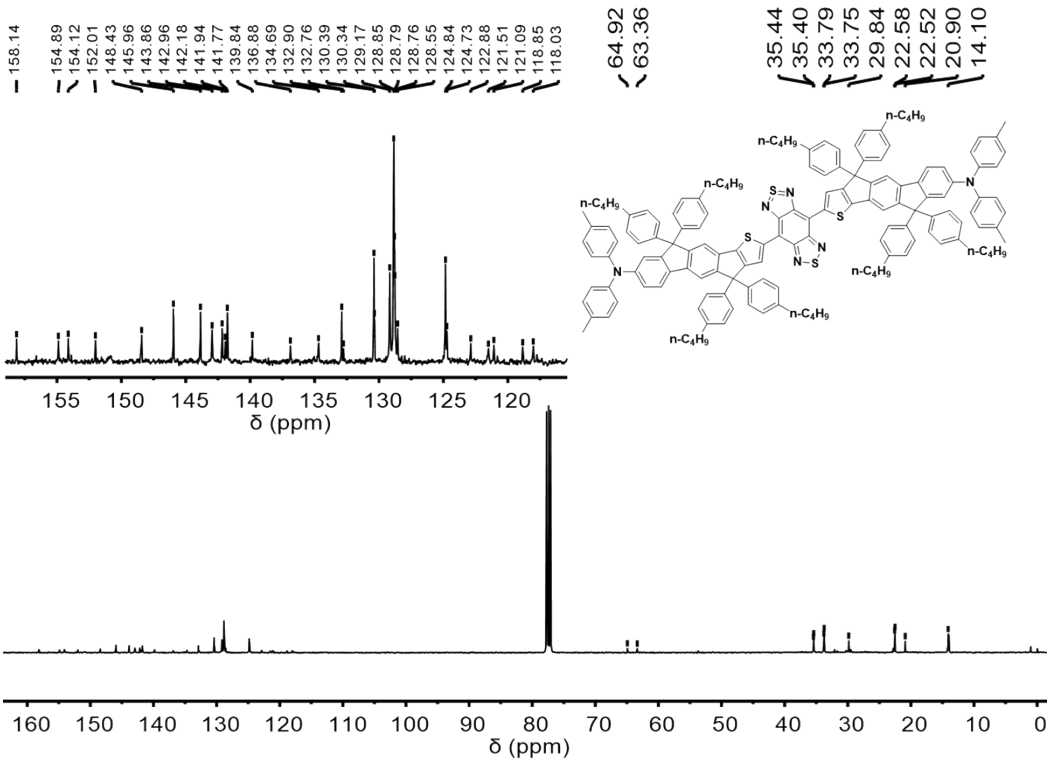

Figure S12. ^{13}C NMR spectrum of BT-BBT.

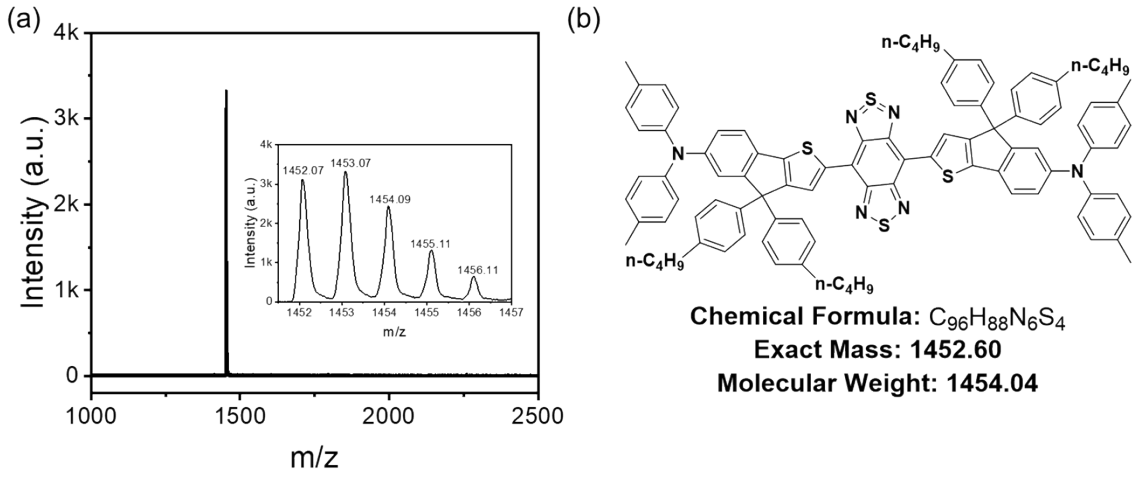

Figure S13. (a, b) MS spectra of T-BBT and molecular information provided by ChemDraw 20.0.

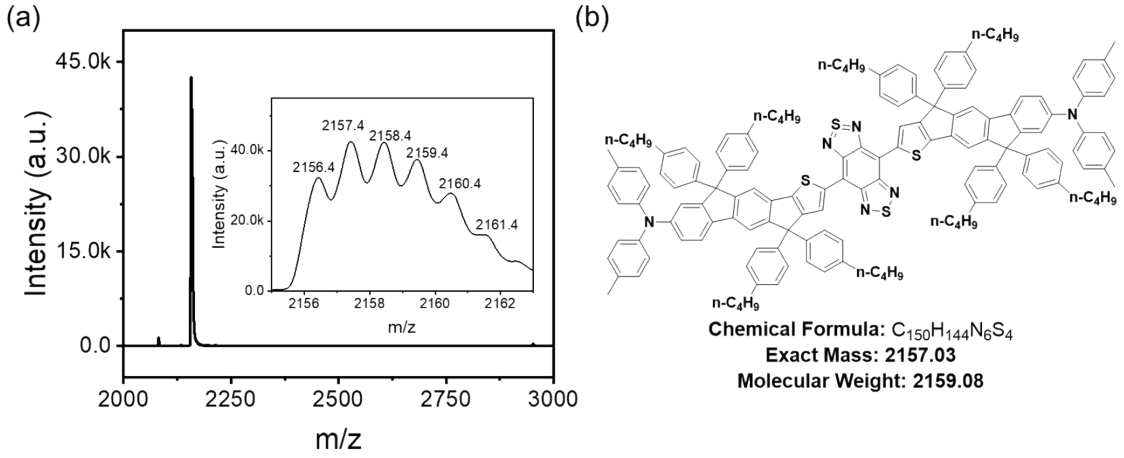

Figure S14. (a, b) MS spectra of BT-BBT and molecular information provided by ChemDraw 20.0.

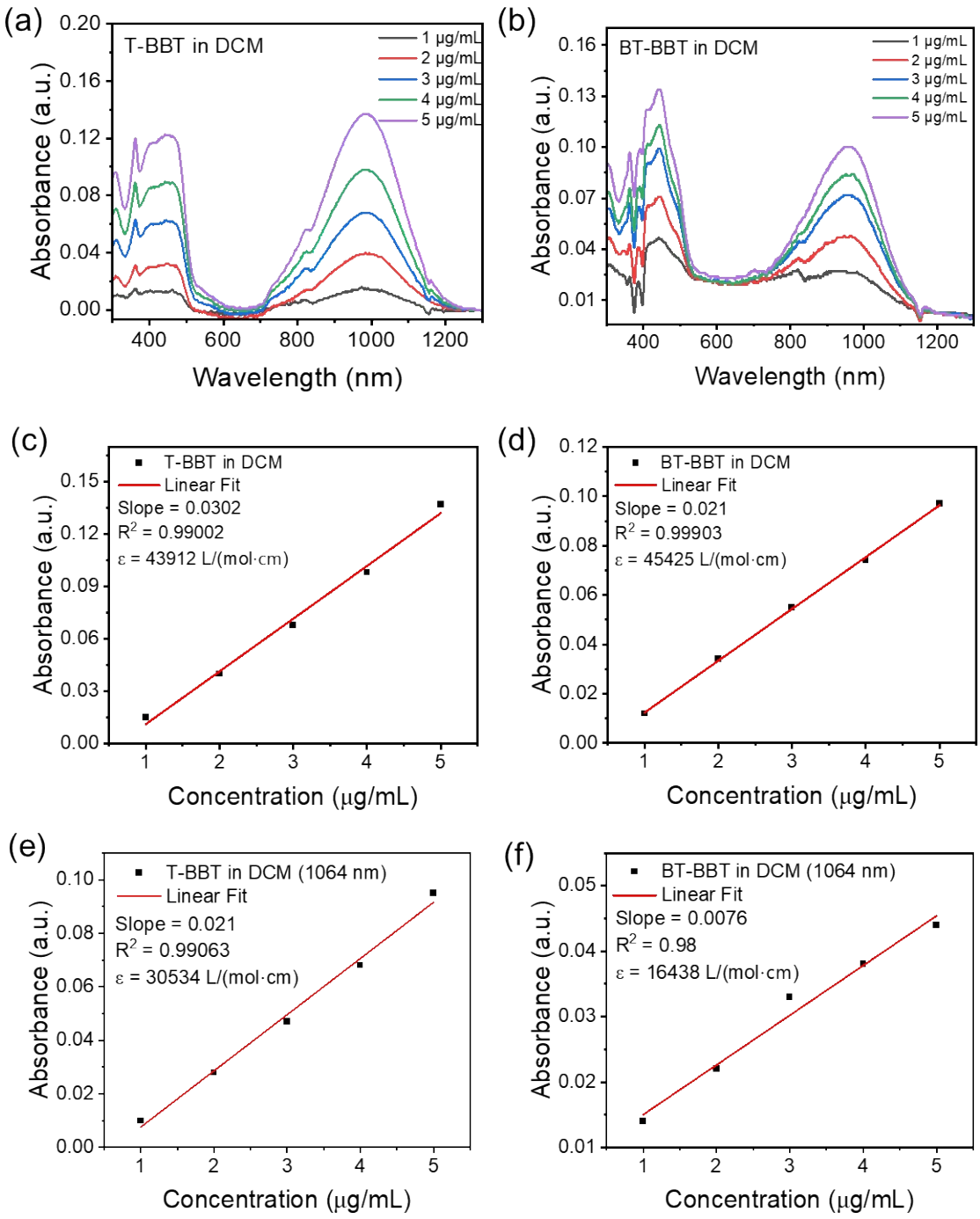

Figure S15. UV-vis absorption spectra of different concentrations T-BBT (a) and BT-BBT (b) in DCM. Absorbance draws scatter plots of concentration and the molar extinction coefficient at maximum absorbance (c, d) and 1064 nm (e, f)calculated by a linear fitting.

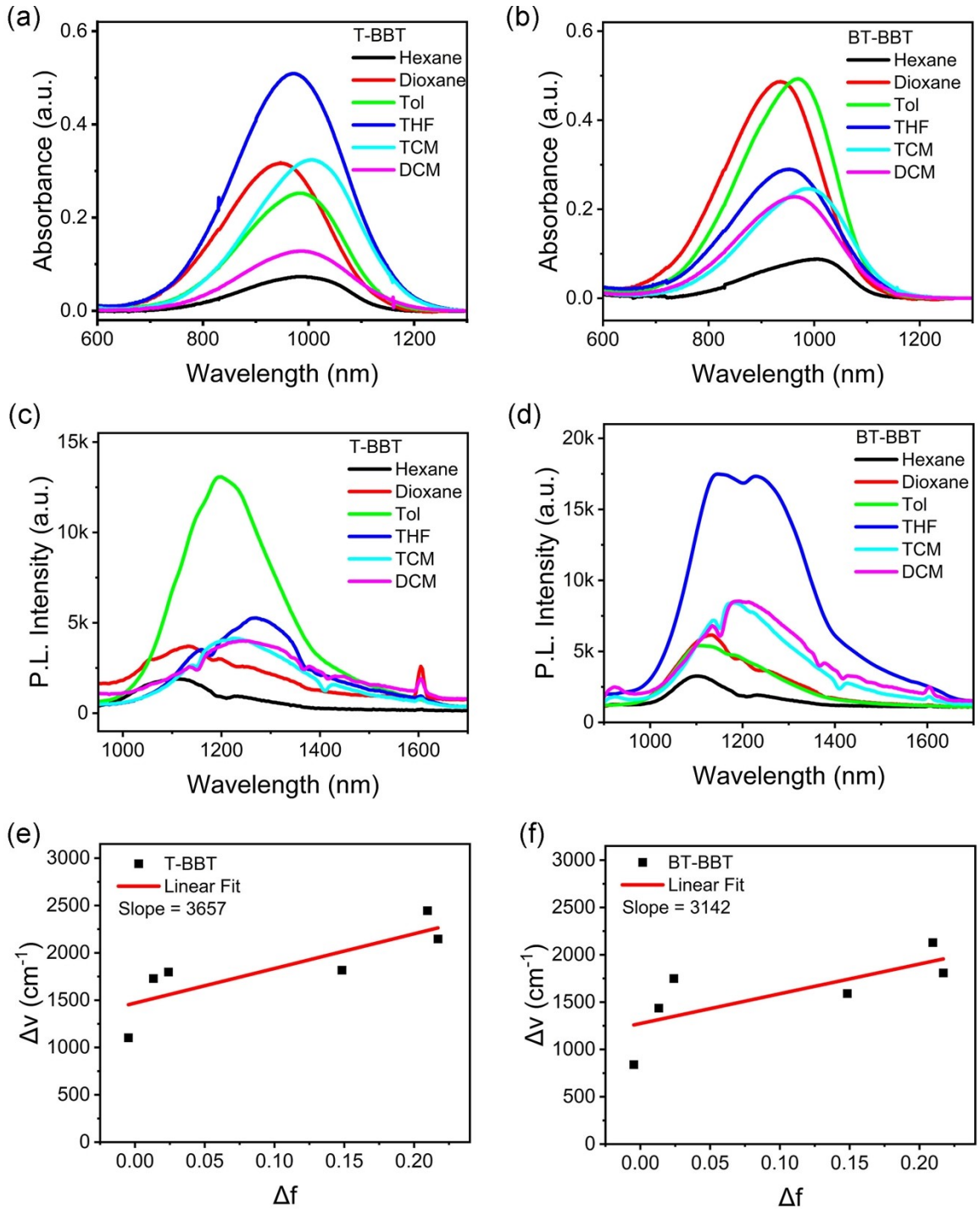

Figure S16. (a-d) UV-vis absorption spectra and fluorescence spectra of T-BBT and BT-BBT in different solvents (Hexane, Dioxane, Tol, THF, TCM, and DCM). Linear fitting of Stokes shifts (Δv) versus solvent orientation polarizability (Δv) parameter (Δf) in different solvents for T-BBT (e) and BT-BBT (f).

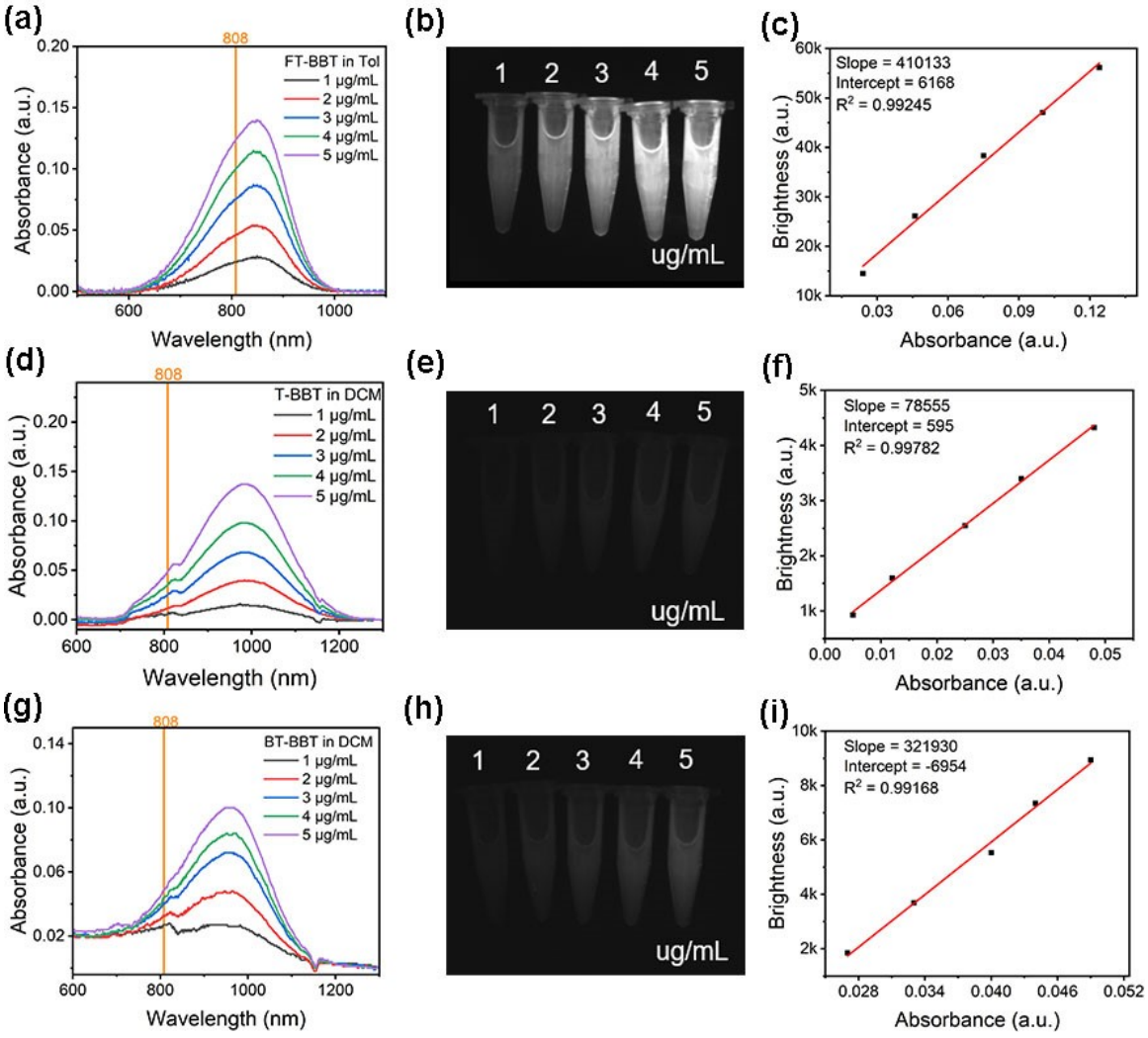

Figure S17. (a, b) UV-vis absorption spectra and NIR-II fluorescence image of FT-BBT in toluene. (c) Fluorescence brightness plotted as a function absorbance at 808 nm for FT-BBT based on the data from (a) and (b). (d, e) UV-vis absorption spectra and NIR-II fluorescence image of T-BBT in DCM. (f) Fluorescence brightness plotted as a function absorbance at 808 nm for T-BBT based on the data from (d) and (e). (g, h) UV-vis absorption spectra and NIR-II fluorescence image of BT-BBT in DCM. (i) Fluorescence brightness plotted as a function absorbance at 808 nm for BT-BBT based on the data from (g) and (h).

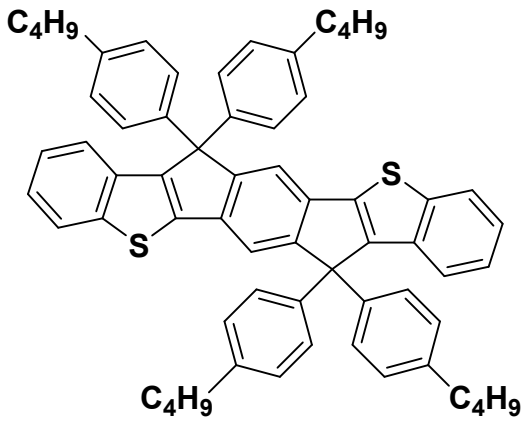

DBT

Figure S18. The chemical structure of DBT.

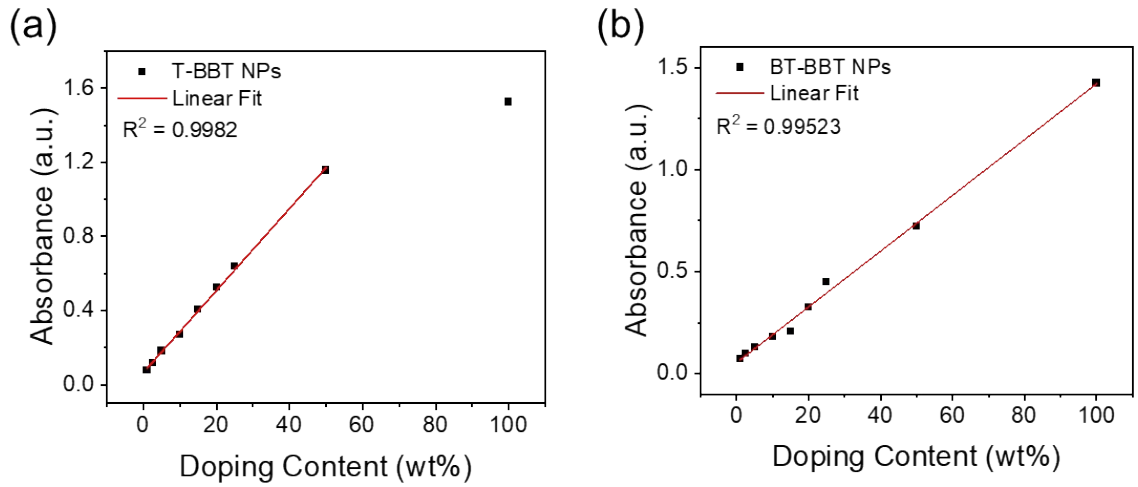

Figure S19. The linear relationship between the maximum absorption and dye doping content (wt%) for T-BBT (b) and BT-BBT (c) NPs. The total mass concentration is 100 μg/mL.

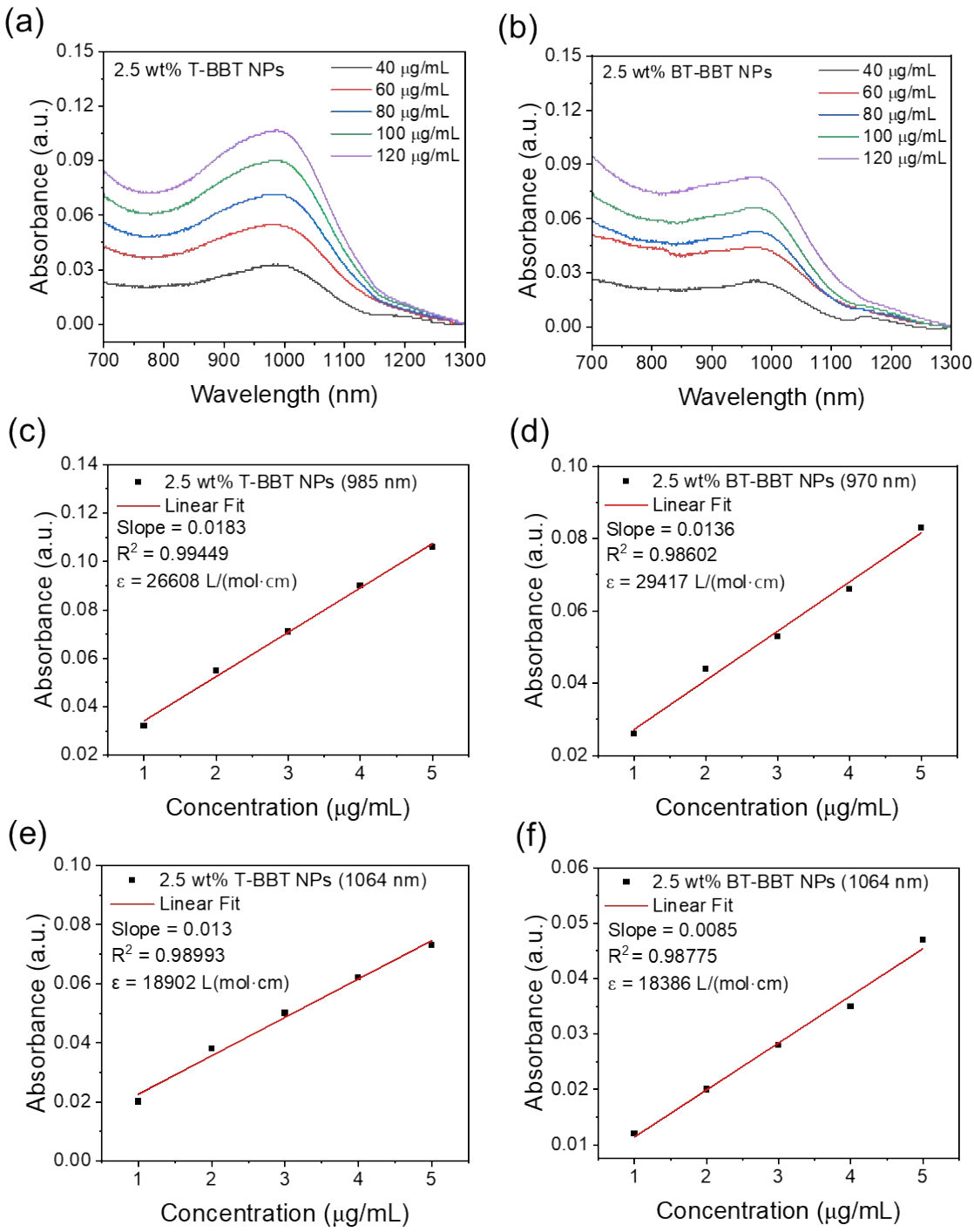

Figure S20. UV-vis absorption spectra of different concentrations 2.5 wt% NPs for T-BBT (a) and BT-BBT (b). Absorbance draws scatter plots of concentration and the molar extinction coefficient at maximum absorbance (c, d) and 1064 nm (e, f)calculated by a linear fitting.

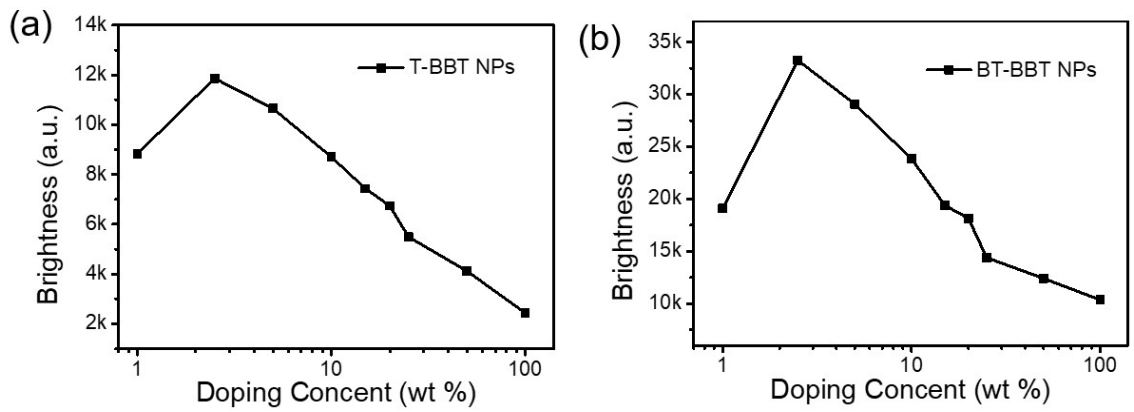

Figure S21. The relation between brightness and doping content for T-BBT (a) and BT-BBT doped NPs (b).

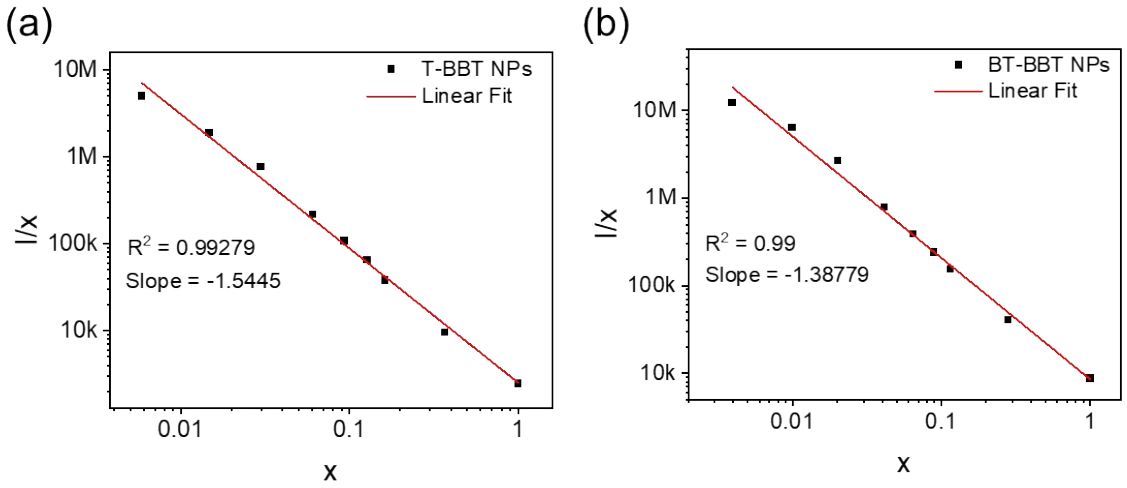

Figure S22. The relation between I/x and x for T-BBT (a) and BT-BBT (b) doping NPs (I: fluorescence intensity, x: molar fraction).

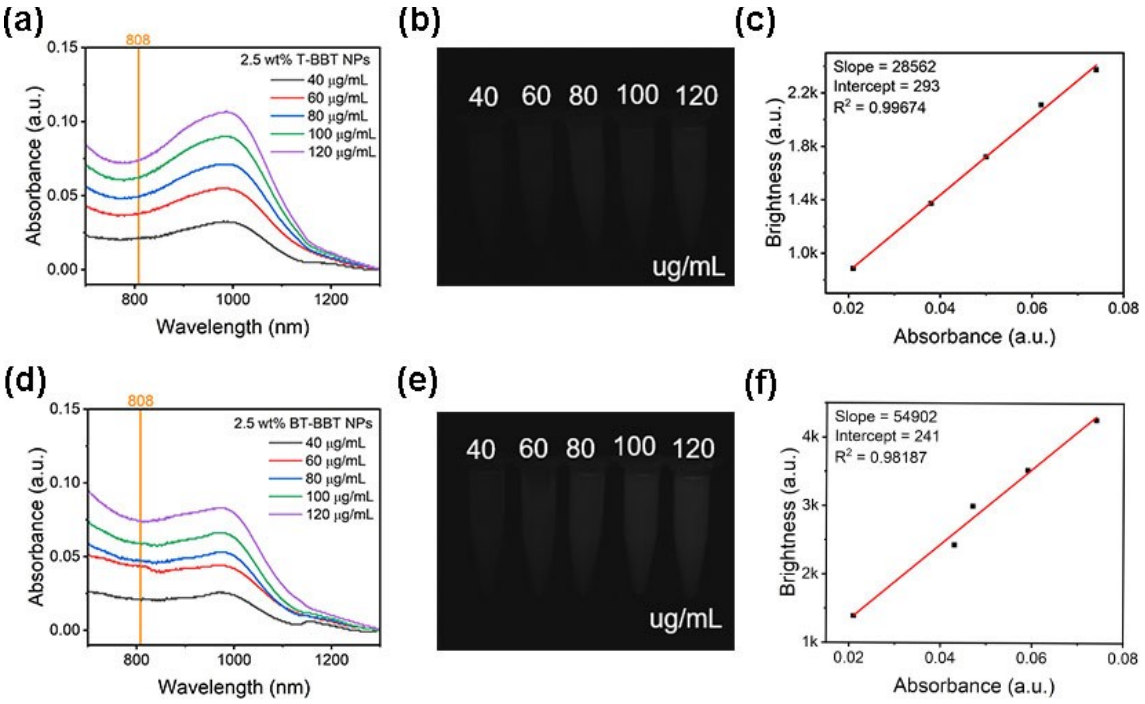

Figure S23. (a, b) UV-vis absorption spectra and NIR-II fluorescence image of T-BBT 2.5 wt% NPs in water. (c) Fluorescence brightness plotted as a function absorbance at 808 nm for T-BBT 2.5 wt% NPs based on the data from (a) and (b). (d, e) UV-vis absorption spectra and NIR-II fluorescence image of BT-BBT 2.5 wt% NPs in water. (f) Fluorescence brightness plotted as a function absorbance at 808 nm for BT-BBT 2.5 wt% NPs based on the data from (d) and (e).

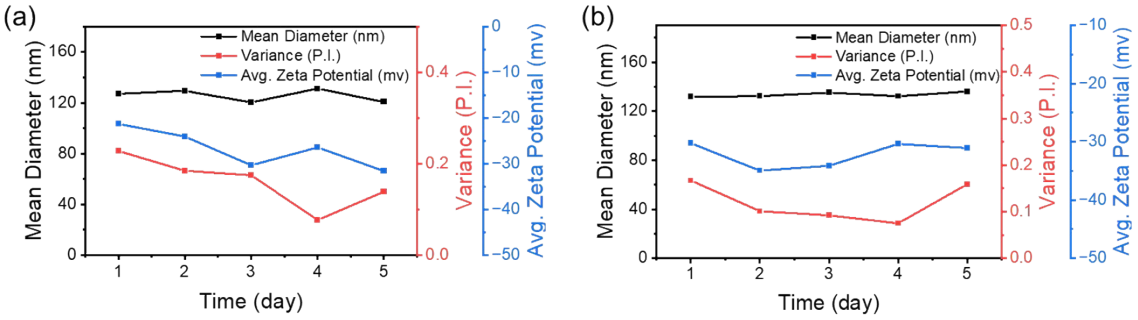

Figure S24. Mean diameter, variance, and average Zeta potential date performed by dynamic light scattering data as a function of storage time of 2.5 wt% doped NPs for T-BBT (a) and BT-BBT (b).

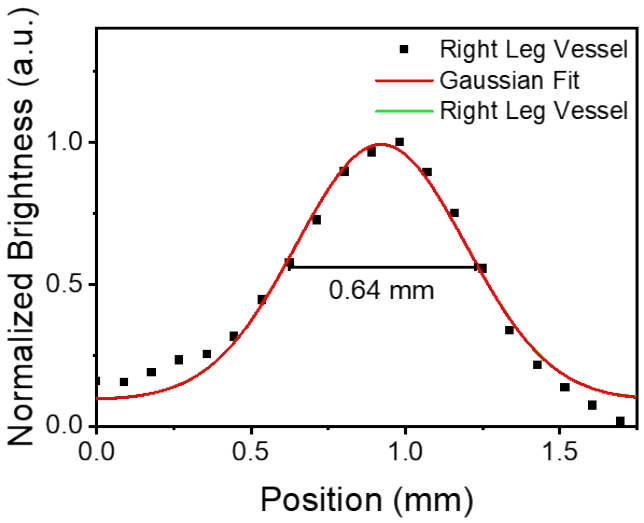

Figure S25. Cross-sectional fluorescence intensity profiles of the right hindlimb vessel were collected and plotted scatter diagrams of position.

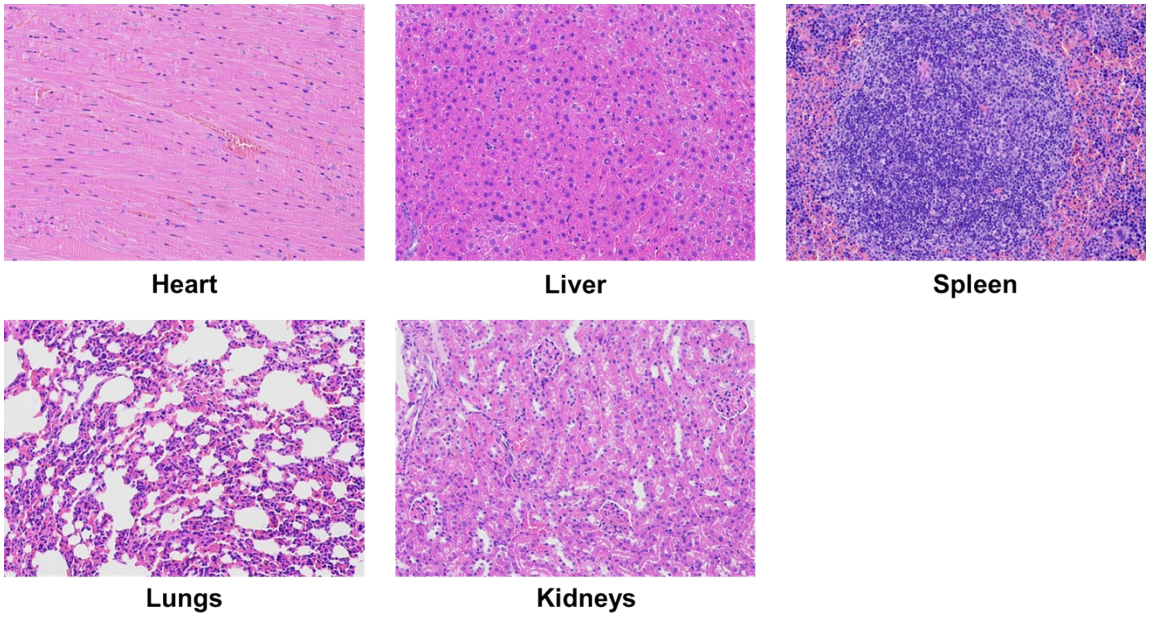

Figure S26. Representative H&E stained images of major organs including heart, liver, spleen, lung, and kidney collected from the 2.5 wt% BT-BBT NPs injected mice after 4 days. The dose of 2.5 wt% BT-BBT NPs was 250 uL (2 mg/mL).

Table S1. Optical data of organic NIR-II fluorophores based on D-A-D structure.

Dyes	λ_{abs} (nm)	λ_{ex} (nm)	$\Delta\upsilon$ (nm/cm^{-1})	ε (10^3 L/(mol·cm))	Φ_f (%)	Ref.
T-BBT	**982**	**1307**	**325/2532**	**43.9**	**1.1**	This work
BT-BBT	**960**	**1246**	**286/2390**	**45.4**	**2.0**	This work
BBTD-1302	942	1302	360/3750	N.A.	2.4	[3]
CH1055-PEG	750	1055	305/3854	N.A.	0.3	[4]
IR-BBEP	741	1050	309/3971	N.A.	0.4	[5]
IR-FTP	828	1047	219/2526	6.95	0.02	[5]
IR-BEMC6P	725	1025	300/4037	N.A.	1.8	[6]
IR-E1	830	1071	240/2702	N.A.	0.7	[7]
IR-FGP	745	1050	305/3899	N.A.	1.9	[8]
IR-FTTP	895	1112	217/2180	7.9	0.1	[9]
IR-FTAP	733	1048	315/4100	5.0	5.3	[9]
IR-BGP6	736	1047	311/4035	8.1	1.5	[10]
IR-FP8P	748	1040	292/3753	13	0.6	[11]
IR-FP0P	732	1043	311/4073	12	0.48	[11]
BTFQ/DMPC	960	1113	153/1431	10.3	0.63	[12]
B2TA	878	1127	249/2516	7.38	0.016	[13]
NK1143-SC12-NPs	966	1096	130/1227	6.9	0.164	[14]
BTBT-BBT	947	1092	145/1402	43	0.97	[1]
BBTD-BTE-PEG	780	1094	314/3680	N.A.	0.004	[15]
IT-TQF	806	1020	214/2603	N.A.	0.04	[16]

Table S2. Host and guest molecules with different mass ratios in nanoparticles

Concentration of T-BBT or BT-BBT	mass (μg, T-BBT or BT-BBT)	mass (μg, host molecular DBT)	Volume (uL, T-BBT or BT-BBT in THF)	Volume (uL, DBT in THF)
1%	50	4950	14.285	495
2.5%	125	4875	35.714	487.5
5%	250	4750	71.428	475
10%	500	4500	142.85	450
15%	750	4250	214.28	425
20%	1000	4000	285.71	400
25%	1250	3750	357.14	375
50%	2500	2500	714.25	250
100%	5000	0	750	0

m (DSPE-mPEG) = 25 mg in each sample.

Table S3. The relative quantum yield of T-BBT, BT-BBT, T-BBT 2.5 wt% NPs, and T-BBT 2.5 wt% NPs. (FT-BBT in toluene as standard sample)

	FT-BBT (Tol)	T-BBT (DCM)	BT-BBT (DCM)	2.5 wt% T-BBT NPs	2.5 wt% B-BBT NPs
Fitted Slope	410133	78555	321930	28562	54902
QYs	19%	3.6%	13.5%	1.1%	2.0%

References

1 C. Ou, L. An, Z. Zhao, F. Gao, L. Zheng, C. Xu, K. Zhang, J. Shao, L. Xie and X. Dong, *Aggregate*, 2023, **4**, e290.

2 I. E. Kolesnikov, D. V. Mamonova, E. Lähderanta, A. V. Kurochkin and M. D.

Mikhailov, *J. Lumin.*, 2017, **187**, 26–32.

3 F. Ye, W. Huang, C. Li, G. Li, W.-C. Yang, S. H. Liu, J. Yin, Y. Sun and G.-F. Yang, *Adv. Therap.*, 2020, **3**, 2000170.

4 A. L. Antaris, H. Chen, K. Cheng, Y. Sun, G. Hong, C. Qu, S. Diao, Z. Deng, X. Hu, B. Zhang, X. Zhang, O. K. Yaghi, Z. R. Alamparambil, X. Hong, Z. Cheng and H. Dai, *Nat. Mater.*, 2016, **15**, 235–242.

5 Q. Yang, Z. Ma, H. Wang, B. Zhou, S. Zhu, Y. Zhong, J. Wang, H. Wan, A. Antaris, R. Ma, X. Zhang, J. Yang, X. Zhang, H. Sun, W. Liu, Y. Liang and H. Dai, *Adv. Mater.*, 2017, **29**, 1654097.

6 R. Tian, H. Ma, Q. Yang, H. Wan, S. Zhu, S. Chandra, H. Sun, D. O. Kiesewetter, G. Niu, Y. Liang and X. Chen, *Chem. Sci.*, 2019, **10**, 326–332.

7 X.-D. Zhang, H. Wang, A. L. Antaris, L. Li, S. Diao, R. Ma, A. Nguyen, G. Hong, Z. Ma, J. Wang, S. Zhu, J. M. Castellano, T. Wyss-Coray, Y. Liang, J. Luo and H. Dai, *Adv. Mater.*, 2016, **28**, 6872–6879.

8 S. Zhu, Q. Yang, A. L. Antaris, J. Yue, Z. Ma, H. Wang, W. Huang, H. Wan, J. Wang, S. Diao, B. Zhang, X. Li, Y. Zhong, K. Yu, G. Hong, J. Luo, Y. Liang and H. Dai, *Proc. Natl. Acad. Sci. U. S. A.*, 2017, **114**, 962–967.

9 Q. Yang, Z. Hu, S. Zhu, R. Ma, H. Ma, Z. Ma, H. Wan, T. Zhu, Z. Jiang, W. Liu, L. Jiao, H. Sun, Y. Liang and H. Dai, *J. Am. Chem. Soc.*, 2018, **140**, 1715–1724.

10 H. Wan, H. Ma, S. Zhu, F. Wang, Y. Tian, R. Ma, Q. Yang, Z. Hu, T. Zhu, W. Wang, Z. Ma, M. Zhang, Y. Zhong, H. Sun, Y. Liang and H. Dai, *Adv. Funct. Mater.*, 2018, **28**, 1804956.

11 H. Ma, C. Liu, Z. Hu, P. Yu, X. Zhu, R. Ma, Z. Sun, C.-H. Zhang, H. Sun, S. Zhu and

Y. Liang, *Chem. Mater.*, 2020, **32**, 2061–2069.

12 P. Chen, F. Qu, S. Chen, J. Li, Q. Shen, P. Sun and Q. Fan, *Adv. Funct. Mater.*, 2022, **48**, 2208463.

13 S. Chen, Y. Pan, K. Chen, P. Chen, Q. Shen, P. Sun, W. Hu and Q. Fan, *Angew. Chem. Int. Ed.*, 2023, **62**, e202215372.

14 S. Liu, W. Xu, X. Li, D.-W. Pang and H. Xiong, *ACS Nano*, 2022, **16**, 17424–17434.

15 J. Li, R. Wang, Y. Sun, P. Xiao, S. Yang, X. Wang, Q. Fan, W. Wu and X. Jiang, *ACS Appl. Mater. Interfaces*, 2021, **13**, 54830–54839.

16 H. Lou, A. Ji, C. Qu, H. Liu, L. Jiang, H. Chen and Z. Cheng, *ACS Appl. Mater. Interfaces*, 2022, **14**, 35454–35465.